ORIGINAL RESEARCH

Vesiculation of biological membrane driven by curvature induced frustrations in membrane orientational ordering

Dalija Jesenek[1]
Šárka Perutková[2]
Wojciech Góźdź[3]
Veronika Kralj-Iglič[4]
Aleš Iglič[2,5]
Samo Kralj[1,6]

[1]Condensed Matter Physics Department, Jožef Stefan Institute, Ljubljana, Slovenia; [2]Laboratory of Biophysics, Faculty of Electrical Engineering, University of Ljubljana, Ljubljana, Slovenia; [3]Department of Complex Systems and Chemical Processing of Information, Institute of Physical Chemistry, Polish Academy of Sciences, Warsaw, Poland; [4]Laboratory of Clinical Biophysics, Faculty of Health Studies, University of Ljubljana, Ljubljana, Slovenia; [5]Laboratory of Clinical Biophysics, Faculty of Medicine, University of Ljubljana, Ljubljana, Slovenia; [6]Department of Physics, Faculty of Natural Sciences and Mathematics, University of Maribor, Maribor, Slovenia

Correspondence: Aleš Iglič
Laboratory of Biophysics,
Faculty of Electrical Engineering,
University of Ljubljana, Tržaška 25,
1000 Ljubljana, Slovenia
Tel +38 614 768 825
Fax +38 614 268 850
Email ales.iglic@fe.uni-lj.si

Abstract: Membrane budding often leads to the formation and release of microvesicles. The latter might play an important role in long distance cell-to-cell communication, owing to their ability to move with body fluids. Several mechanisms exist which might trigger the pinching off of globular buds from the parent membrane (vesiculation). In this paper, we consider the theoretical impacts of topological defects (frustrations) on this process in the membranes that exhibit global in-plane orientational order. A Landau–de Gennes theoretical approach is used in terms of tensor orientational order parameters. The impact of membrane shapes on position and the number of defects is analyzed. In studied cases, only defects with winding numbers $m = \pm 1/2$ appear, where we refer to the number of defects with $m = 1/2$ as defects, and with $m = -1/2$ as anti-defects. It is demonstrated that defects are attracted to regions with maximal positive Gaussian curvature, K. On the contrary, anti-defects are attracted to membrane regions exhibiting minimal negative values of K. We show on membrane structures exhibiting spherical topology that the coexistence of regions with $K > 0$ and $K < 0$ might trigger formation of defect–anti-defect pairs for strong enough local membrane curvatures. Critical conditions for triggering pairs are determined in several demonstrative cases. Then the additionally appeared anti-defects are assembled at the membrane neck, where $K < 0$. Consequent strong local fluctuations of membrane constituent anisotropic molecules might trigger membrane fission neck rupture, enabling a membrane fission process and the release of membrane daughter microvesicles (ie, vesiculation).

Keywords: structural transitions, topological defects, membrane microvesicles, membrane curvature, membrane fission, vesiculation

Introduction

The influence of various parameters on biological membrane structures and shapes is of interest for medicine, biology, and physics. Changes in membrane shapes are linked with several cellular processes of vital biological importance. For example, the membrane budding process plays an important role in cell-to-cell communication. If a relatively long tubular bud is formed, it typically initially explores its neighboring surrounding. By way of such a dynamic process, it might attach to an adjacent cell, forming the so-called tunneling nanotube.[1–5] If a small globular bud is created, it might pinch off from the parent cell converting to a microvesicle.[6–9] Micro- and nanovesicles are more or less free to move with body fluids and can reach distant cells. Interactions with these vesicles might enable an effective long distance cell-to-cell communication system. They can transport genetic material, cytokines, prions, infective particles, and so on. In this way, they might spread inflammation, infection, and contribute to cancer progression.[6]

Methods have been developed to isolate microvesicles from blood in order to exploit them as diagnostic and therapeutic tools,[10] and as indicators of homeostasis.[11] As these methods might replace invasive procedures and suppress diseases at their origin,[12] it is of interest to understand the mechanisms of formation of nanotubular protrusions and microvesicles (vesiculation). Such configurational changes might be provoked by varying external conditions (temperature, pressure, concentration), by changes in effective elasticity by adhering nanoparticles or colloids, or by some other process.[13–16] Furthermore, if a membrane exhibits an in-plane orientational order,[17] the membrane configuration might be strongly affected by the presence of topological defects (TDs) (frustrations) in the orientational degree of the in-plane membrane ordering. These effects are addressed in the present paper. We will analyze the possible TD-driven changes in membrane configurations (shape), which might trigger the pinching-off of a tubular or spherical bud from the parent membrane, or play a role in other membrane fission (vesiculation) processes.

Theories of TDs are strongly interdisciplinary because they rely on the topology which neglects system-specific details.[18] For example, the first comprehensive theory of the coarsening of TDs was developed in cosmology in order to explain the coarsening dynamics of the Higgs field in the early universe.[19] Furthermore, several studies on defects in orientational ordering have been carried out in various condensed matter systems (superconductors, superfluids, liquid crystals) in order to reveal fundamental features related to the structure of our universe.[20]

TDs in the ordering of membrane components are, in most cases, unavoidable due to topological reasons,[21,22] if the membrane exhibits a tangential (in-plane) orientational ordering. The latter may be found on a local or global level. In giant unilamellar vesicles containing cholesterol and sphingolipid mixtures, the regions of the liquid ordered phase, L_o, are distributed in the liquid disordered predominant phase.[23] In cells, membrane rafts are supposed to be in the L_o phase.[24] Global orientational ordering has been also observed in giant unilamellar vesicles at low temperatures where lipids are in the gel phase (L_β) or in some other ordered phase. Chiral membrane constituents may also exhibit an orientational order.[25,26] Furthermore, it may also occur due to embedded anisotropic proteins,[27–32] or due to self-organized filament networks.[33] Local orientational order can also arise from the alignment of anisotropic membrane components in localized, highly curved parts of the membrane.[34,35]

A pioneering study assessing the impact of in-plane ordering on membrane shape was performed by MacKintosh and Lubensky[17] using a mean-field theory. This and more recent investigations have demonstrated that the coupling between in-plane ordering of membrane anisotropic components and membrane mechanical properties could trigger transitions between spherical and cylindrical shapes of vesicles or vesicle protrusions.[32,36] In these studies, it is assumed that two TDs are enforced at antipodal poles, preserving the global axial symmetry. However, recent theoretical studies have revealed that such symmetric configurations could be realized only under specific conditions. A study on nematic liquid crystalline shells performed by Vitelli and Nelson[37] revealed that in equilibrium, four defects appear forming a tetrahedron lattice structure in elastically isotropic cases, structured as such to maximize their mutual separation. However, in relatively large elastic anisotropies,[22,38] or structures in which Gaussian curvature exhibits a relatively strong spatial dependence,[22,39] various defect structures might appear exhibiting a different number of defects.

In this paper, we will study the influence of TDs on different axisymmetric membrane shapes where orientational ordering and defects are allowed to break this symmetry. In particular, we will investigate the impacts of this TD in in-plane membrane orientational ordering on membrane budding initiated fission (vesiculation) processes. We will use a minimal model, which will allow us to study the impact of membrane curvature on the number and position of TDs (ie, frustrations in in-plane orientational ordering). The outline of the paper is as follows: in section 2, we will present the theoretical background. Results are presented in section 3. In the last section, we will summarize our results. Some technical details are given in the Supplementary materials section.

Theoretical background

In this section, we will first define TDs in membrane orientational ordering and their key topological characteristics. Next, we will introduce our minimal model, through which we will study membrane shapes exhibiting different configuration of TDs.

Characterization of defects

We consider membrane systems exhibiting in-plane orientational ordering, which is at the mesoscopic level locally determined by the director field, $\bar{n}$. In other words, to every point on the surface, we can assign vector $\bar{n}$ as having a direction in which membrane constituents are oriented at a given point. However, the vector head and tail are indistinguishable

$(\pm \bar{n})$, thus orientation is represented with bars instead of arrows (see Figure 1). We say the director field has so called head-to-tail symmetry. For example, this is a characteristic feature of the nematic ordering encountered in nematic liquid crystalline phases.[18,40] TDs refer to points or lines, where the director field is not uniquely defined,[18] as illustrated in Figure 1. They can arise either as: (1) unavoidable due to topological reasons (ie, they are formed because of specific surface geometry); (2) they can be stabilized energetically;[41] or (3) they are formed temporarily after a fast enough symmetry that breaks the phase transition.[19,20,42] It should be noted that the local free energy costs of introducing TD are in general relatively large. Therefore, in most cases, systems do not exhibit TDs;[19,20,42] however, due to topological reasons, one cannot get rid of an isolated TD if the director field on any surface that encloses the defect is fixed. One can decrease the number of TDs only if a pair of different defects (the so-called defect and anti-defect) annihilate each other.[43,44] One can assign a topological charge, q, to each defect, which is a topological invariant.[18] In two dimensional systems (2D), to which we will henceforth restrict the current discussion, the topological charge is equivalent to the winding number, m. In liquid crystals, it is also referred to as the Frank index.[18,40] The winding number is determined by the orientational field surrounding TD. It counts the total amount of change in the orientation of $\bar{n}$ on encircling TD in a clockwise manner (using an arbitrary path), divided by 2π. If TD exists, then m equals a half integer or an integer. Absence of a single defect corresponds to $m = 0$.

In Figure 2, schematic plots of simple TDs bearing $m = 1/2$, $m = -1/2$, $m = 1$ and $m = -1$ are shown. TDs exhibiting $m > 0$ and $m < 0$ are commonly referred to as defects and anti-defects, respectively. Note that TDs, in most cases, behave in
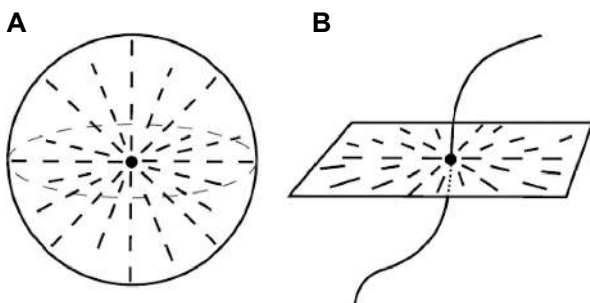

Figure 1 Schematic presentation of topological defects in orientational order in three dimensional space. Here, (**A**) points to the defect and (**B**) points to the line defect. In the latter case, we show the orientational order only in a planar cross-section for visual reasons. The orientation at a given point is represented with the bar, where the head and tail are indistinguishable. However, at the point of origin of the defects, the director field is not uniquely defined (ie, there is no preferred direction) and thus the defect origin is marked with a dot.
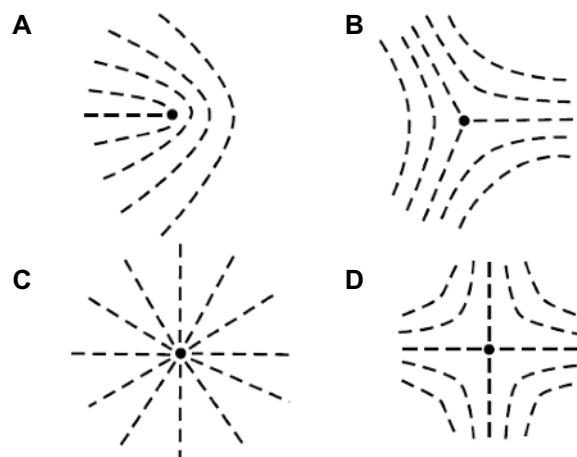

Figure 2 Schematic presentations of topological defects in orientational ordering in the two dimensional plane. Dashed curves indicate the spatial distribution of the director field. With a point we mark the origin of a defect. In a real system, and at the defect origin, the locally melted (ie, ordinary liquid) phase is realized. (**A**) represents $m = 1/2$; (**B**) represents $m = -1/2$; (**C**) represents $m = 1$; and (**D**) represents $m = -1$.

a similar way as electrically charged particles or fundamental particles in particle physics, bearing some quantized charge in general.[45] Namely, TDs of opposite winding numbers attract each other and can annihilate into a defectless state, while defects with same value of m repel each other.

The total sum of winding numbers (m_{tot}) of all TDs residing on a closed surface (eg, a membrane) is determined by Poincare's[46] theorem. The author claims that m_{tot} must equal the Euler-Poincare characteristic, $\chi = 2(1-g)$, of the surface. The integer, g, is the genus of the surface, reflecting the number of "handles" that the surface contains. An object with the spherical topology is characterized by $g = 0$, and consequently $m_{tot} = 2$. The topological number, χ, is determined by the Gaussian curvature, K, of the surface. The spatial dependence of K could have strong impacts on position and even on the number of TDs. Simple XY-type modeling suggests that a positive value of (negative) K attracts TDs with a positive (negative) value of m.[47] Furthermore, surfaces exhibiting both negative and positive Gaussian curvature might trigger unbinding of topological pairs, defect–anti-defect.

Model

We model a membrane as a 2D film possessing in-plane orientational ordering. The local shape of the membrane is described by a curvature tensor, $\underline{C}$. Its eigenvalues, C_1 and C_2, are the principal curvatures along the orthogonal directions within the membrane. The local mean curvature, H, and the Gaussian curvature, K, can be expressed as:

$$H = \frac{1}{2} Tr\underline{C} = \frac{1}{2}\left(C_1 + C_2\right) \tag{1}$$

and

$$K = Det\underline{C} = C_1 C_2 \qquad (2)$$

here, Tr and *Det* stand for the trace and determinant operation, respectively.

For the latter purpose, we also define the normalized average mean curvature as:

$$\langle h \rangle = R_0 \langle H \rangle, \qquad (3)$$

where,

$$\langle H \rangle = \frac{1}{A} \int H dA \qquad (4)$$

and

$$R_0 = (A/4\pi)^{1/2} \qquad (5)$$

are calculated, where A is a given membrane area and V is the enclosed volume. We also define the vesicle relative volume as $v = V/V_0$, which is a ratio of the vesicle enclosed volume to the volume (V_0) of the sphere with the same area (A) as the given vesicle.

For a given axial-symmetric membrane structure, we study a degree of in-plane membrane orientational ordering using a simple 2D phenomenological Landau–de Gennes-type model.[22] The degree of ordering is expressed in terms of the tensor order parameter:

$$\underline{Q} = \lambda \left(\bar{n} \otimes \bar{n} - \bar{n}_\perp \otimes \bar{n}_\perp \right) \qquad (6)$$

here, the orthogonal unit vectors ($\bar{n}$ and $\bar{n}_\perp$) are eigenvectors of $\underline{Q}$, and the corresponding eigenvalues are $\lambda \in [0,1/2]$ and $-\lambda$, respectively. In this parametrization, $\bar{n}$ plays the role of the director field that was introduced in the previous subsection. The normal orientation of the local membrane is determined by $\bar{v} = \bar{n} \times \bar{n}_\perp$. The maximal degree of orientational order corresponds to $\lambda = 1/2$. On the other hand, the orientational order vanishes (ie, it is melted) when $\lambda = 0$. For example, points exhibiting $\lambda = 0$ in a system exhibiting orientational order can reveal locations of TDs. The core structure of a defect is roughly given by the biaxial order parameter length, ξ_b. Within the core, the degree of ordering is substantially depressed with respect to regions where elastic distortions are relatively weak. Note that local order could also be generally melted in the absence of TDs due to high enough local temperatures or strong enough local elastic distortions.

We express the free energy of the system in terms of $\underline{Q}$ and $\underline{C}$. Only the most essential terms are introduced in order to demonstrate the phenomenon of interest. In simulations, we assume that $\underline{C}$ is a primary and $\underline{Q}$ is a secondary parameter

of the model. Therefore, we assume that a membrane shape is primarily dictated by the curvature tensor. We restrict shapes exhibiting axial symmetry. For a given membrane shape, we then determined the orientational field distribution, allowing for the departure from axial symmetry. Our model is described in more detail in the Supplementary materials (parametrization and free energy density).

Simulation results

In the following section we present the impact of membrane (ie, cell or vesicle) curvature on the number and distribution of TDs in the membrane possessing of in-plane orientational ordering. Different axial symmetric shapes of spherical topology (ie, roughly spoken, closed shapes with no holes such as spheres, oblate, and prolate shapes) are considered. They are characterized by the appropriate choice of the normalized average membrane mean curvature, $\langle h \rangle$, and the vesicle relative volume, v. Orientational field configurations were obtained numerically using our model, which is described in the Supplementary materials (parametrization and free energy density). Of particular interest is to determine the conditions in which TDs might trigger or facilitate membrane fission processes. We restricted the conditions to low enough temperatures where orientational ordering is spontaneously formed.

For the geometries studied, TDs are unavoidably formed due to topological constraints enforcing $m_{tot} = 2$. At defect sites, $\bar{n}$ is not uniquely defined and corresponding high elastic penalties give rise to local melting. Therefore, the positions of defects are well determined by points where $\lambda = 0$. This is illustrated in Figure 3 where we display the degree of ordering on a spherical membrane. The corresponding director field configuration is shown in Figure 4A. In our simulations, such spherical geometries correspond to the relative volume, $v = 1.0$.

In Figure 3A, the degree of ordering (λ) is superimposed on the membrane structure. Defect sites are clearly visible in Figure 3B where we plot the spatial evolution along the planar coordinate system (φ, ϑ). Here the azimuthal ($\varphi \in [0,2\pi]$) and zenithal ($\vartheta \in [0,\pi]$) angles determine the meridians and parallels of the sphere, respectively. Within a sphere, the Gaussian curvature is spatially homogeneous. For the chosen conditions (ie, elastically isotropic medium), four TDs with a winding number ($m = 1/2$) occupy the vertices of a tetrahedron. In such a way, this repels the TDs from bearing the same topological charge to maximize their mutual separation. A more detailed analysis was provided elsewhere.[22]

Our interest is to estimate the conditions that enable the development of qualitatively different defect configurations
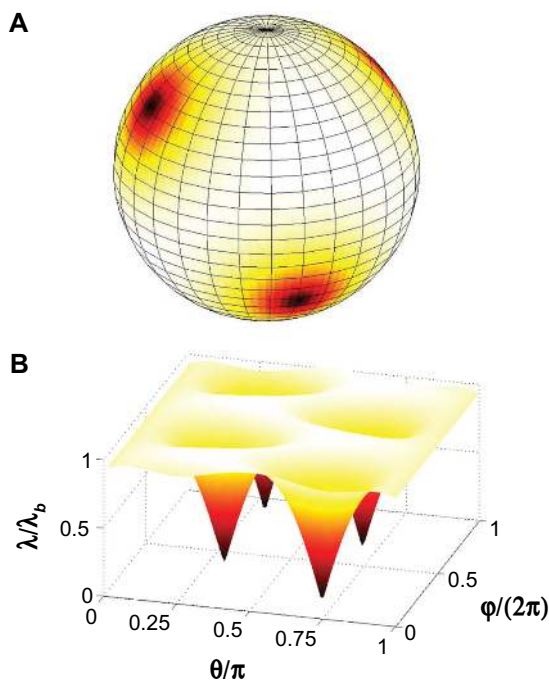
Figure 3 Defects on a spherical membrane structure. (**A**) The normalized order parameter variations on a spherical membrane where four defects with a topological charge ($m = 1/2$) appear. The total topological charge is $m_{tot} = 2$. (**B**) The orientational order is plotted on the (φ, ϑ) plane, where coordinates φ and ϑ determine the meridians and parallels of a sphere, respectively. At the point of the defect origins, it holds that $\lambda/\lambda_b = 0$, where λ_b stands for the degree of orientational order in bulk. Relative volume is $v = 1.0$ and $R/\xi_b = 3.46$.

for a given (spherical) topology of vesicles (cells). This could be achieved by varying the Gaussian curvature of a vesicle's shape. Namely, in addition to fixing the total winding number (m_{tot}) of a membrane, K might also influence the relative position and number of defects if it exhibits strong enough spatial variations. A typical vesicle/cell geometry that enables
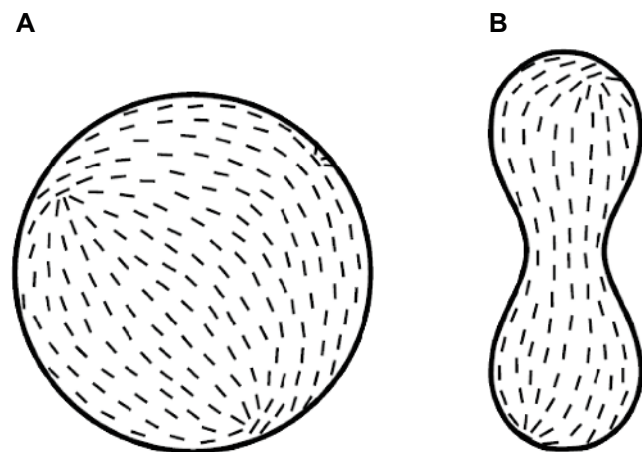

Figure 4 Schematic figures showing typical director fields on membrane shapes. The director field configurations for (**A**) a spherical membrane (see also Figure 3A) and (**B**) a membrane possessing two beads (see also Figure 6B) are shown. The defects have a topological charge ($m = 1/2$).

such a phenomenon is shown in Figure 5A. It possesses both regions with positive and negative Gaussian curvature, as depicted in Figure 5B. If regions exhibiting different signs of K coexist, the unbinding of defect pairs might be triggered, as simple XY-modeling (using only $\bar{n}$ as a variational parameter) suggests.[47] In cases studied, a pair consists of a defect with $m = 1/2$ and an anti-defect with $m = -1/2$.

A typical unbinding process (ie, process at which defect–anti-defect pairs are formed) is demonstrated in Figure 6 where we show the sequence of vesicle shapes corresponding to increasing values of $\langle h \rangle$ for $v = 0.695$. This value of v enables formation of vesicle shape composed of two equal spherical or spheroidal parts (beads) during vesicle shape transformation. Namely in this case, it holds that the number of beads is equal to v^{-2} (see also Iglic et al).[48] For such geometries, we found that for $\langle h \rangle < \langle h \rangle^{(c)}(v)$, four defects in in-plane membrane ordering exist for isotropic orientational elastic properties, as demonstrated in Figure 6A and B. The corresponding director field configuration for Figure 6B is show in Figure 4B. The quantity, $\langle h \rangle^{(c)}(v = 0.695) \sim 1.312$, stands for a critical value of $\langle h \rangle$ for a given value of v, at which defect unbinding is realized. In this process, two pairs of defects appear (this is demonstrated in Figure 6C). Because negative (positive) curvature attracts defects with negative (positive) signs of m, two anti-defects are assembled at the neck of the structure, where $K < 0$. The remaining six defects are collected in regions where $K > 0$. Therefore, our
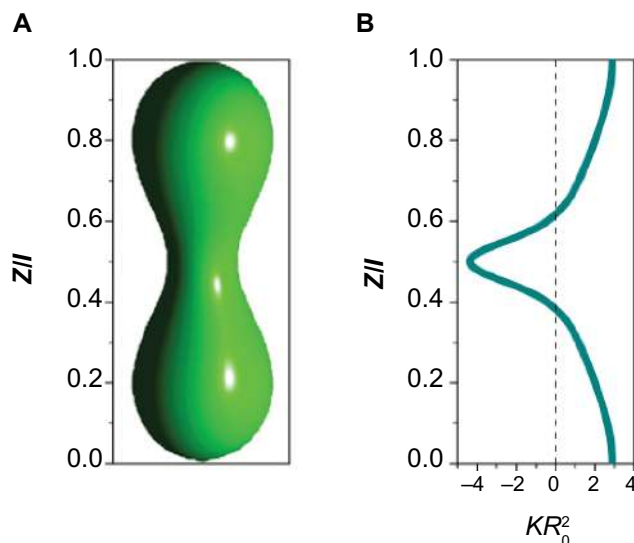

Figure 5 The Gaussian curvature, K. For the membrane shape shown in (**A**) we plotted the variations of normalized Gaussian curvature, KR_0^2, along the symmetry axis-z shown in (**B**). At the neck, K is negative; therefore, it attracts defects with a negative topological charge. On the other hand, defects with a positive topological charge tend to assemble at regions where $K > 0$. The membrane shape was calculated for $\langle h \rangle = 1.275$ and $v = 0.695$. l stands for the length of the membrane along the z axis and $R_0 = (A/4\pi)^{1/2}$, where A is the membrane area.
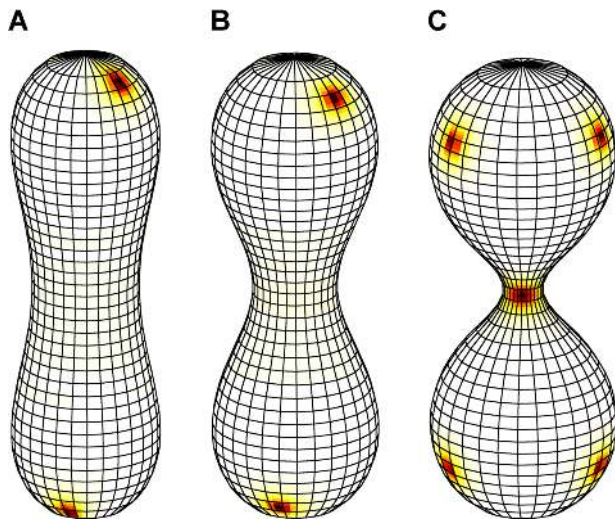
Figure 6 The number and position of defects on a membrane possessing two beads. For (**A**) $\langle h \rangle = 1.250$ and (**B**) $\langle h \rangle = 1.275$, where $\langle h \rangle$ is the normalized average mean curvature, the membrane structure exhibits four defects with a topological charge where $m = 1/2$. (**C**) If $\langle h \rangle$ is large enough, the defect–antidefect pairs could be created. When $\langle h \rangle = 1.353$, there exist eight defects: two anti-defects ($m = -1/2$) are formed at the neck where $K < 0$, and three defects ($m = 1/2$) are noted within each bead where $K > 0$. The total topological charge of membranes for all cases is $m_{tot} = 2$. The shapes were calculated for $v = 0.695$. The defects were obtained for $t = -0.03$ and $R/\xi_b = 13.86$.

modeling confirms the predictions of a simple XY-type model that defects and anti-defects assemble at regions exhibiting maximal and minimal negative values of K, respectively.[47]

Some further vesicle/cell shapes possessing lower symmetry, and which are commonly observed experimentally (membrane budding),[36] are shown in Figure 7. In Figure 7A we plotted defect configuration (lateral distribution of defects) superimposed onto a vesicle geometric shape. The
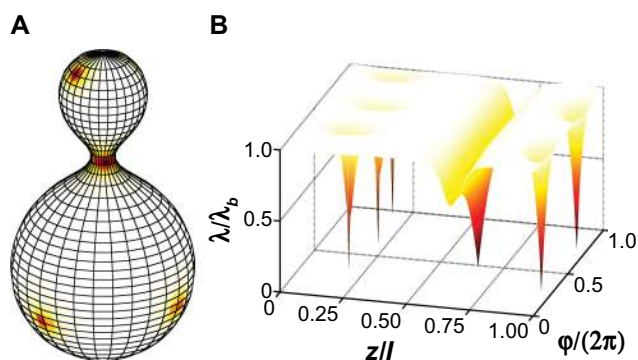

Figure 7 The number and position of the defects on a membrane composed of beads of different sizes. (**A**) The normalized order parameter variations on the membrane structure, and (**B**) the corresponding orientational order in the (φ, z)-plane. At the point of the defect origins, orientational order is melted ($\lambda = 0$). Coordinates φ and z determine the meridians and parallels of the cylindrically symmetric shape. The membrane structure possesses three defects at the bottom bead and two defects at the top bead, each bearing $m = 1/2$. At the neck, one antidefect ($m = -1/2$) is located, so the total topological charge of the structure is $m_{tot} = 2$. l stands for the membrane length. The membrane configuration is calculated for $v = 0.80$, $\langle h \rangle = 1.287$, $t = -0.03$, and $R/\xi_b = 15.59$, where R stands for the radius at the bottom spherical part.

corresponding profile in the rectangular parameter space $\{\varphi, z\}$ (Figure 7B) reveals the positions of TDs. Three defects were assembled at the larger, spherical part at the bottom, and two were assembled at the smaller upper part. In such a manner, repelling interactions among defects are minimized. One anti-defect is located at the neck of the structure; therefore, $m_{tot} = 2$.

In Figure 8, the vesicle shapes exhibiting three beads connected by necks are shown. Upon increasing the curvature, the number of TDs equals ten (Figure 8A), 12 (Figure 8B), and 14 (Figure 8C). Note that in all cases, the total charge equals $m_{tot} = 2$ because all of the shapes exhibit a spherical topology. In all shown configurations, four defects reside within the bottom spherical part of the vesicle, which enables the relatively large mutual separations of repelling defects. In Figure 8A, an additional six TDs (ie, three defects pairs; $m = -1/2$, $m = 1/2$) are formed due to strong enough negative curvatures at the bottom neck. Three anti-defects are localized at the bottom neck of the structure. The corresponding defects are assembled within the upper two beads (one within the middle bead and two at the top bead) in regions exhibiting $K > 0$. On the other hand, the upper neck, which exhibits lower curvature, does not possess TDs.

In Figure 8B, a vesicle shape possessing 12 defects is shown. In this case, an additional pair (defect–anti-defect)
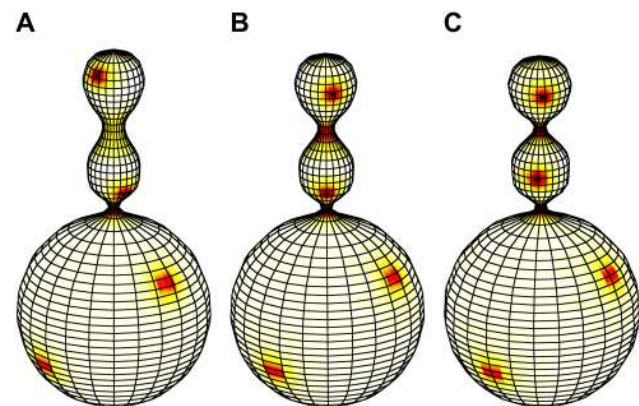

Figure 8 The number and position of defects on membrane shapes composed of three beads. Defects and anti-defects are characterized by $m = 1/2$ and $m = -1/2$, respectively. For (**A**) $\langle h \rangle = 1.438$, the membrane structure has four defects at the bottom bead, one in the middle and two at the upper bead. At the lower thinner neck, three anti-defects are assembled, and none are in the thicker part of the upper neck. On increasing the normalized average mean curvature, additional topological defect–antidefect pairs appear. For (**B**) $\langle h \rangle = 1.453$, the vesicle exhibits 12 defects. An additional antidefect appears in the upper neck, and the corresponding defect is placed at the upper bead, which now possesses three defects. For (**C**) $\langle h \rangle = 1.462$, there are four defects at the bottom bead, two defects at the middle bead, and one and three at the upper bead. Three anti-defects are located at the lower neck and two anti-defects are located at the upper neck. The total topological charge in all membranes is $m_{tot} = 2$. The membrane shapes were calculated for $v = 0.80$. The defects were obtained for $t = -0.03$ and $R/\xi_b = 13.86$, where R stands for the radius of the bottom spherical part.

is triggered at the upper neck of the structure. Consequently, the neck is now occupied by a newly created anti-defect. Its partner defect is located at the top bead, which now possesses three defects. Finally, in Figure 8C we show a structure possessing 14 TDs. In this case, the bottom, middle, and top regions with $K > 0$ possess four, two, and three defects, respectively. The corresponding five anti-defects are assembled at the bottom (three anti-defects) and top (two anti-defects) of the neck.

Discussion and conclusion

In this paper we considered the biological membranes with in-plane orientational ordering.[17,25–35,49] In such systems, TDs (frustrations) in orientational order might appear. In fact, they are unavoidable in topologies which are different from toroidal ones.[46] Cores of defects exhibited relatively strong local elastic distortions, which might play an important role in biological processes. In this paper we focused on membrane curvature-driven unbinding of TDs in vesicles of spherical topology alone (see Figures 6–8). A simple 2D Landau–de Gennes-type phenomenological approach was used where the degree of in-plane vesicle ordering was described in terms of the tensorial order parameter.[22] In the cases studied, TDs characterized by the winding number $m = 1/2$ or $m = -1/2$ appeared,[18,40] which are commonly referred to as defects and anti-defects, respectively. The unbinding process, in which pairs of defects–anti-defects are formed, are enabled if: (1) a relatively strong local curvature exists; and (2) if a membrane possesses regions exhibiting both positive and negative Gaussian curvature. The first condition is necessary to lower the cost of forming TDs, and the second condition is needed to separate TDs to prevent their annihilation (the defect is attracted to the region where $K > 0$ and the anti-defect is attracted to the region where $K < 0$). This unbinding mechanism was first predicted using a simple XY-type model in which only orientations of interacting constituents were taken into account.[47] Our simulations, in which the degree of ordering is also included, confirms the robustness of the phenomenon.

We simulated defect textures for vesicle shapes that are reminiscent of shapes that have been observed in previous experiments,[6,50,51] and which are close to limiting shapes (shape transition points).[50,52] Neck regions in these shapes possess negative Gaussian curvatures surrounded by regions exhibiting a positive Gaussian curvature. We found that when a neck curvature exceeds a certain threshold value pairs of defects–anti-defects are formed where anti-defects are localized at the necks.

Next, we will discuss the possible impact of defect unbinding on biological membrane or vesicle transformations if these configurations that exhibit in-plane membrane orientational ordering. For illustration purposes, we confined our interest to the shapes shown in Figure 6. In our simulations, these shapes are enabled by varying the average membrane curvature, which could be triggered in a real biological system via changes of relevant control parameters (eg, temperature or osmotic pressure). In Figure 9 we schematically depicted the different possible shape transformations that are commonly observed in such configurations.[6,50–57] Generally in a fission process (ie, vesiculation), a final system exhibits lower or same membrane Helfrich bending energy. However, the fission process generally requires that an energy barrier has to be overcome. This might be triggered or facilitated by the unbinding of TDs if the parent system exhibits in-plane membrane orientational ordering. Namely, a fission process requires a thin enough neck that fulfills both of the necessary
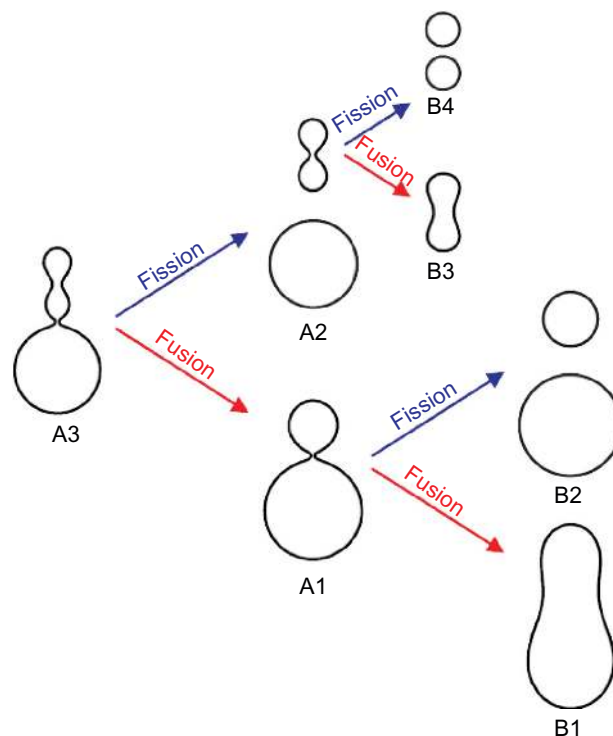

Figure 9 Schematic figure showing possible scenarios of a shape transformation of the vesicle (cell) with a protrusion. The terminal membrane neck connecting the terminal bead to the large parent vesicle is usually always much thinner than the other necks interconnecting the beads in the protrusion.[36] The stable thin terminal membrane neck may transit (after fluctuations following the creation of the orientational ordering defect in the neck) into a state with a diminished number of beads (one bead less) following the fusion of the terminal daughter vesicle (transitions A3 → A1), including the fusion of the single (ie, the last) bead (transition A1 → B1). Alternatively, the thin neck may be disrupted following the fission of the whole membrane protrusion (transitions A3 → A2 or A1 → B2), and later fission of the detached daughter vesicle (transition A2 → B4).[16,50,58]

conditions discussed above for the unbinding of TDs. In the cores of TDs, strong fluctuations in membrane orientation ordering take place. Consequently, interactions among the neighboring membrane constituents are weakened. The resulting softer structure could further enable pronounced shape fluctuations. Consequently, the fission neck molecular reorganization could be triggered, enabling the opening of the thin membrane of the neck, leading to the fission (ie, vesiculation process).

In Figure 10 we show a typical budding formation with a necklace-type budding process.[59] One sees that with time, the necks separating the spherically-shaped buds progressively narrow (Figure 10A and B). In Figure 10C, a chain of buds is pinched-off. Finally, in Figure 10D, the necklace decays into separate microvesicles. If in-plane membrane orientational ordering exists, the rupturing of narrow necks can be facilitated by anti-defects assembled at narrow enough necks. The existence of in-plane orientation at the narrow neck was discussed by Kralj-Iglič et al.[34] The creation of anti-defects in the narrow neck may induce strong fluctuations, which can then cause the neck to rupture, thus pinching off of the small microvesicle.

The proposed mechanism responsible for the pinching off of the membrane bud from the parent membrane can also explain the observed differences in the stability and shape dynamics of the prolate giant unilamellar vesicles in the liquid disordered phase (L_α) and in the liquid ordered phase (L_o).[51] In the experiment, a small vesicle bud was connected by a neck to a parent vesicle. The bud was then aspirated from the parent vesicle membrane. In the case of the L_α phase, the daughter vesicle remains connected to the parent vesicle by a thin long tube, while in the case of the L_o phase, the thin tube is disrupted and the daughter vesicle is released from the parent membrane.

These observations support our model, where the strong in-plane orientational order of the membrane in the L_o phase induces the detachment of the daughter vesicle from its parent vesicle because of the unbinding of TDs (ie, the formation of defect–anti-defect pairs) in the narrow neck leading to strong local membrane fluctuations and neck rupture. Unlike what occurred in the L_o phase, the neck rupture was not observed in L_α phase where the membrane orientational ordering was supposed to be considerably weaker, and thus the unbinding of the defect in this region was not very likely to occur.

Acknowledgments

Disclosure

The authors report no conflicts of interest in this work.

Figure 10 Vesiculation of a giant phospholipid vesicle (POPC, cardiolipin, cholesterol in 2:2:1 molar ratios). After the addition of phosphate buffered saline to a suspension of vesicles, the tubular bud (**A**) exhibited undulations (**B**), detached itself from the mother vesicle (**C**), and decomposed into separate spherical vesicles, which were free to migrate away from the mother vesicle (**D**).
Notes: The bar = 10 μm. Adapted from *Chem Phys Lipids*. 2007;150(1):49–57, Urbanija J, Tomsic N, Lokar M, et al. Coalescence of phospholipid membranes as a possible origin of anticoagulant effect of serum proteins. Copyright 2007, with permission from Elsevier.[59]
Abbreviation: POPC, palmitoyl-oleoyl-phosphatidylcholine.

References

1. Rustom A, Saffrich R, Markovic I, Walther P, Gerdes HH. Nanotubular highways for intercellular organelle transport. *Science*. 2004;303(5660): 1007–1010.
2. Watkins SC, Salter RD. Functional connectivity between immune cells mediated by tunneling nanotubules. *Immunity*. 2005;23(3): 309–318.
3. Vidulescu C, Clejan S, O'connor KC. Vesicle traffic through intercellular bridges in DU 145 human prostate cancer cells. *J Cell Mol Med*. 2004; 8(3):388–396.
4. Veranic P, Lokar M, Schütz GJ, et al. Different types of cell-to-cell connections mediated by nanotubular structures. *Biophys J*. 2008;95(9): 4416–4425.
5. Kabaso D, Lokar M, Kralj-Iglič V, Veranič P, Iglič A. Temperature and cholera toxin B are factors that influence formation of membrane nanotubes in RT4 and T24 urothelial cancer cell lines. *Int J Nanomedicine*. 2011;6:495–509.
6. Kralj-Iglic V. Stability of membranous nanostructures: a possible key mechanism in cancer progression. *Int J Nanomedicine*. 2012;7: 3579–3596.
7. Hägerstrand H, Isomaa B. Vesiculation induced by amphiphiles in erythrocytes. *Biochim Biophys Acta*. 1989;982(2):179–186.
8. Junkar I, Šuštar V, Frank M, et al. Blood and synovial microparticles as revealed by atomic force and scanning electron microscope. *Open Autoimmun J*. 2009;1(9):50–58.
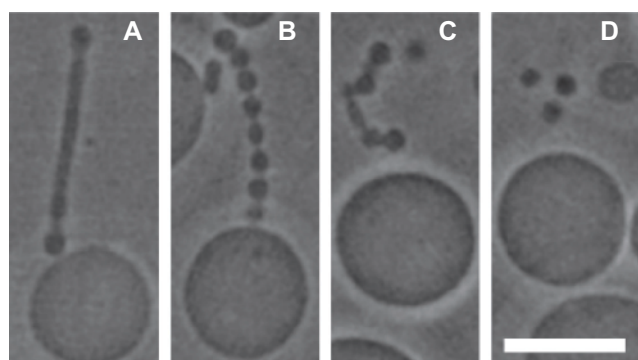
9. Mrvar-Brecko A, Sustar V, Jansa V, et al. Isolated microvesicles from peripheral blood and body fluids as observed by scanning electron microscope. *Blood Cells Mol Dis*. 2010;44(4):307–312.

10. Suštar V, Bedina-Zavec A, Štukelj R, et al. Nanoparticles isolated from blood: a reflection of vesiculability of blood cells during the isolation process. *Int J Nanomedicine*. 2011;6:2737–2748.

11. Suštar V, Bedina-Zavec A, Stukelj R, et al. Post-prandial rise of microvesicles in peripheral blood of healthy human donors. *Lipids Health Dis*. 2011;10:47.

12. Sustar V, Jansa R, Frank M, et al. Suppression of membrane microve-siculation – a possible anticoagulant and anti-tumor progression effect of heparin. *Blood Cells Mol Dis*. 2009;42(3):223–227.

13. Cullis PR, Hope MJ, Tilcock CP. Lipid polymorphism and the roles of lipids in membranes. *Chem Phys Lipids*. 1986;40(2–4):127–144.

14. Farsad K, De Camilli P. Mechanisms of membrane deformation. *Curr Opin Cell Biol*. 2003;15(4):372–381.

15. Zimmerberg J, Kozlov MM. How proteins produce cellular membrane curvature. *Nat Rev Mol Cell Biol*. 2006;7(1):9–19.

16. McMahon HT, Gallop JL. Membrane curvature and mechanisms of dynamic cell membrane remodelling. *Nature*. 2005;438(7068): 590–596.

17. MacKintosh FC, Lubensky TC. Orientational order, topology, and vesicle shapes. *Phys Rev Lett*. 1991;67(9):1169–1172.

18. Mermin ND. The topological theory of defects in ordered media. *Rev Mod Phys*. 1979;51(3):591–648.

19. Kibble TWB. Topology of cosmic domains and strings. *J Phys A Math Gen*. 1976;9(8):1387–1398.

20. Zurek WH. Cosmological experiments in superfluid helium? *Nature*. 1985;317(6037):505–508.

21. Kamien RD. The geometry of soft materials: a primer. *Rev Mod Phys*. 2002;74(4):953–971.

22. Kralj S, Rosso R, Virga EG. Curvature control of valence on nematic shells. *Soft Matter*. 2011;7(2):670–683.

23. Bacia K, Schwille P, Kurzchalia T. Sterol structure determines the sepa-ration of phases and the curvature of the liquid-ordered phase in model membranes. *Proc Natl Acad Sci U S A*. 2005;102(9):3272–3277.

24. Simons K, Gerl MJ. Revitalizing membrane rafts: new tools and insights. *Nat Rew Mol Cell Biol*. 2010;11(10):688–699.

25. Helfrich W, Prost J. Intrinsic bending force in anisotropic membranes made of chiral molecules. *Phys Rev A*. 1988;38(6):3065–3068.

26. Oda R, Huc I, Schmutz M, Candau SJ, MacKintosh FC. Tuning bilayer twist using chiral counterions. *Nature*. 1999;399(6736):566–569.

27. Tian A, Baumgart T. Sorting of lipids and proteins in membrane cur-vature gradients. *Biophys J*. 2009;96(7):2676–2688.

28. Baumgart T, Capraro BR, Zhu C, Das SL. Thermodynamics and mechanics of membrane curvature generation and sensing by proteins and lipids. *Annu Rev Phys Chem*. 2011;62:483–506.

29. Fournier JB. Nontopological saddle-splay and curvature instabilities from anisotropic membrane inclusions. *Phys Rev Lett*. 1996;76(23): 4436–4439.

30. Kralj-Iglic V, Svetina S, Zeks B. Shapes of bilayer vesicles with mem-brane embedded molecules. *Eur Biophys J*. 1996;24(5):311–321.

31. Kralj-Iglič V, Heinrich V, Svetina S, Žekš B. Free energy of closed mem-brane with anisotropic inclusions. *Eur Phys J B*. 1999;10(1):5–8.

32. Kabaso D, Bobrovska N, Góźdź W, et al. On the role of membrane anisotropy and BAR proteins in the stability of tubular membrane structures. *J Biomech*. 2012;45(2):231–238.

33. Köhler S, Schaller V, Bausch AR. Collective dynamics of active cytoskeletal networks. *PLoS One*. 2011;6(8):e23798.

34. Kralj-Iglič V, Babnik B, Gauger DR, May S, Iglič A. Quadrupolar ordering of phospholipid molecules in narrow necks of phospholipid vesicles. *J Stat Phys*. 2006;125(3):727–752.

35. Nagle JF, Tristram-Nagle S. Structure of lipid bilayers. *Biochim Biophys Acta*. 2000;1469(3):159–195.

36. Kralj-Iglič V, Iglič A, Gomišček G, Sevšek F, Arrigler V, Hägerstrand H. Microtubes and nanotubes of a phospholipid bilayer membrane. *J Phys A Math Gen*. 2002;35(7):1533–1549.

37. Vitelli V, Nelson DR. Nematic textures in spherical shells. *Phys Rev E Stat Nonlin Soft Matter Phys*. 2006;74(2):021711.

38. Lopez-Leon T, Koning V, Devaiah KBS, Vitelli V, Fernandez-Nieves A. Frustrated nematic order in spherical geometries. *Nat Phys*. 2011;7(5):391–394.

39. Skacej G, Zannoni C. Controlling surface defect valence in colloids. *Phys Rev Lett*. 2008;100(19):197802.

40. Virga EG. *Variational Theories for Liquid Crystals*. 1st ed. London, UK: Chapman and Hall; 1994.

41. Bradač Z, Kralj S, Žumer S. Molecular dynamics study of nematic structures confined to a cylindrical cavity. *Phys Rev E Stat Phys Plasmas Fluids RElat Interdiscip Topics*. 1998;58(6):7447–7454.

42. Bradač Z, Kralj S, Žumer S. Early stage domain coarsening of the isotropic-nematic phase transition. *J Chem Phys*. 2011;135(2):024506.

43. Svetec M, Kralj S, Bradac Z, Zumer S. Annihilation of nematic point defects: pre-collision and post-collision evolution. *Eur Phys J E Soft Matter*. 2006;20(1):71–79.

44. Ambrozic M, Kralj S, Sluckin TJ, Zumer S, Svensek D. Annihilation of edge dislocations in smectic-A liquid crystals. *Phys Rev E Stat Nonlin Soft Matter Phys*. 2004;70(5 Pt 1):051704.

45. Repnik R, Mathelitsch L, Svetec M, Kralj S. Physics of defects in nematic liquid crystals. *European Journal of Physics*. 2003;24(4):481–491.

46. Poincare H. Mémoire sur les courbes définies par une équation différentielle. *J Math Pures Appl*. 1886;2(4):151–217. French.

47. Vitelli V, Turner AM. Anomalous coupling between topological defects and curvature. *Phys Rev Lett*. 2004;93(21):215301.

48. Iglic A, Kralj-Iglic V, Majhenc J. Cylindrical shapes of closed lipid bilayer structures correspond to an extreme area difference between the two monolayers of the bilayer. *J Biomech*. 1999;32(12): 1343–1347.

49. Uchida N. Dynamics of orientational ordering in fluid membranes. *Phys Rev E Stat Nonlin Soft Matter Phys*. 2002;66(4 Pt 1):040902.

50. Iglič A, Kralj-Iglič V. Budding of liposomes – role of intrinsic shape of membrane constituents. In: Leitmannova Liu A, editor. *Advances in Planar Lipid Bilayers and Liposomes*, Vol 4. Amsterdam: Elsevier; 2006:253–279.

51. Tanaka T, Sano R, Yamashita Y, Yamazaki M. Shape changes and vesicle fission of giant unilamellar vesicles of liquid-ordered phase membrane induced by lysophosphatidylcholine. *Langmuir*. 2004; 20(22):9526–9534.

52. Urbanija J, Babnik B, Frank M, et al. Attachment of beta 2-glycoprotein I to negatively charged liposomes may prevent the release of daugh-ter vesicles from the parent membrane. *Eur Biophys J*. 2008;37(7): 1085–1095.

53. Leirer C, Wunderlich B, Myles VM, Schneider MF. Phase transi-tion induced fission in lipid vesicles. *Biophys Chem*. 2009;143(1–2): 106–109.

54. Andes-Koback M, Keating CD. Complete budding and asymmetric division of primitive model cells to produce daughter vesicles with different interior and membrane compositions. *J Am Chem Soc*. 2011;133(24):9545–9555.

55. Franke T, Leirer CT, Wixforth A, Dan N, Schneider MF. Phase-transition- and dissipation-driven budding in lipid vesicles. *Chemphyschem*. 2009;10(16):2852–2857.

56. Döbereiner HG, Käs J, Noppl D, Sprenger I, Sackmann E. Budding and fission of vesicles. *Biophys J*. 1993;65(4):1396–1403.

57. Käs J, Sackmann E. Shape transitions and shape stability of giant phospholipid vesicles in pure water induced by area-to-volume changes. *Biophys J*. 1991;60(4):825–844.

58. Hurley JH, Hanson PI. Membrane budding and scission by the ESCRT machinery: it's all in the neck. *Nat Rev Mol Cell Biol*. 2010;11(8): 556–566.

59. Urbanija J, Tomsic N, Lokar M, et al. Coalescence of phospholipid membranes as a possible origin of anticoagulant effect of serum proteins. *Chem Phys Lipids*. 2007;150(1):49–57.

60. Góźdź W. Spontaneous curvature induced shape transformations of tubular polymersomes. *Langmuir*. 2004;20(18):7385–7391.

Supplementary materials
Videos
Video 1 http://youtu.be/E_Mjss0Lu8Q Variation of positions and number of defects on a membrane possessing two beads on increasing the normalized average mean curvature $\langle h \rangle$ from $\langle h \rangle = 1.271$ to $\langle h \rangle = 1.360$.

Video 2 http://youtu.be/xU5UhBUmUZU Variation of the number and position of defects for membrane shapes composed of three beads on increasing $\langle h \rangle$ from $\langle h \rangle = 1.438$ to $\langle h \rangle = 1.456$.

Video 3 http://youtu.be/oZGrZZ5cgEk Shape transformation of a vesicle with bead-like chain protrusion in a stepwise process corresponding to a decrease of the vesicle $\langle h \rangle$ from 1.41 to 1.31.

Parametrization and free energy density

The vesicle profile is parameterized by the angle, θ, of the tangent to the profile with the plane that is perpendicular to the axis of rotation, as a function of the arc length, s (see Figure S1).[60] The parametric equations of the vesicle profile are given by the following equations:

$$z(s) = \int_0^s ds' \cdot \sin \theta(s'), \tag{1}$$

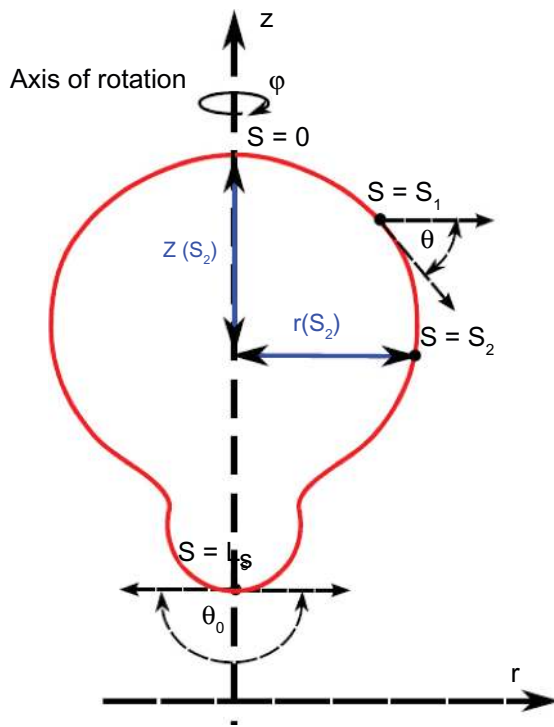$$r(s) = \int_0^s ds' \cdot \cos \theta(s'). \tag{2}$$

Figure S1 Schematic representation of a profile in the arc length parametrization.
Note: $\theta(s)$ is a parametrization, where s is the arc length, and L_s is the length of the profile.

In the three-dimensional Euclidean space, the vector describing the points on a surface of revolution is given by:

$$\bar{R} = \{r(s) \cos \varphi, r(s) \sin \varphi, z(s)\}. \tag{3}$$

The angle of rotation φ and the arc length, s, are coordinates determining the membrane surfaces. In order to calculate the principal curvatures (C_1 and C_2) on the surface, we define the metric tensor g:

$$\underline{g} = \begin{bmatrix} \dfrac{\partial \bar{R}}{\partial s} \cdot \dfrac{\partial \bar{R}}{\partial s} & \dfrac{\partial \bar{R}}{\partial \varphi} \cdot \dfrac{\partial \bar{R}}{\partial s} \\ \dfrac{\partial \bar{R}}{\partial s} \cdot \dfrac{\partial \bar{R}}{\partial \varphi} & \dfrac{\partial \bar{R}}{\partial \varphi} \cdot \dfrac{\partial \bar{R}}{\partial \varphi} \end{bmatrix} = \begin{bmatrix} G & F \\ F & E \end{bmatrix} = \begin{bmatrix} 1 & 0 \\ 0 & r(s)^2 \end{bmatrix}, \tag{4}$$

where $\partial \bar{R}/\partial s = \{\cos \varphi \cdot \cos \theta(s), \sin \varphi \cdot \cos \theta(s), \sin \theta(s)\}$, $\partial \bar{R}/\partial \varphi = \{-\sin \varphi \cdot r(s), \cos \varphi \cdot r(s), 0\}$. The unit normal $\bar{\nu}$ is given by $\bar{\nu} = (\partial \bar{R}/\partial s \times \partial \bar{R}/\partial \varphi)/\sqrt{\det(\underline{g})} = \{-\cos \varphi \cdot \sin \theta(s), -\sin \varphi \cdot \sin \theta(s), \cos \theta(s)\}$.

The second fundamental form, J, is given by:

$$\underline{J} = \begin{bmatrix} \dfrac{\partial^2 \bar{R}}{\partial s^2} \cdot \bar{\nu} & \dfrac{\partial^2 \bar{R}}{\partial s \partial \varphi} \cdot \bar{\nu} \\ \dfrac{\partial^2 \bar{R}}{\partial \varphi \partial s} \cdot \bar{\nu} & \dfrac{\partial^2 \bar{R}}{\partial \varphi^2} \cdot \bar{\nu} \end{bmatrix} = \begin{bmatrix} L & M \\ M & N \end{bmatrix} \tag{5}$$

The curvature tensor $\underline{C}$ is then:

$$\underline{C} = \underline{g}^{-1} \underline{J} = \begin{bmatrix} \dfrac{d\theta(s)}{ds} & 0 \\ 0 & \dfrac{\sin(\theta(s))}{r(s)} \end{bmatrix}. \tag{6}$$

Most of the vesicle shapes considered in this paper are calculated for the values of parameters close to limiting values and are resembling limiting shapes, which are mainly determined by the area-to-volume ratio of the vesicles (for example, see the paper by Kralj-Iglič et al).[34] For reasons of simplicity, the shapes of vesicles used in the present study are determined in an independent procedure of the curvature energy minimization of the isotropic membrane. These shapes are then used to study the topological defects of the membrane possessing in-plane orientational ordering.

Orientational ordering on a membrane surface is parameterized as:[22]

$$\underline{Q} = q_0 \left(\bar{e}_1 \otimes \bar{e}_1 - \bar{e}_2 \otimes \bar{e}_2 \right) + q_m \left(\bar{e}_1 \otimes \bar{e}_2 - \bar{e}_2 \otimes \bar{e}_1 \right) \tag{7}$$

The unit vectors $\bar{e}_1$ and $\bar{e}_2$ represent the local orthonormal basis, where $\bar{e}_1$ and $\bar{e}_2$ point along the meridians ($\varphi = constant.$) and parallels ($s = constant.$) of a surface of revolution, respectively. The degree of orientational ordering is described by q_0 and q_m, where $\lambda = \sqrt{q_0^2 + q_m^2}$. Note that the meridians and parallels are also lines of principal curvatures.

The orientational degree of freedom is determined via minimization of the free energy $f = f_c + f_e$, where f_c and f_e determine order parameter condensation and elastic contribution. In the simplest form they are expressed as:[22]

$$f_c = \frac{A_0 t}{2} Tr\underline{Q}^2 + \frac{B}{4} Tr\underline{Q}^4, \tag{8}$$

$$f_e = \frac{k_e}{2} \left|\nabla_s \underline{Q}\right|^2. \tag{9}$$

Here, $t = (T - T_c)/T_c$ stands for the reduced temperature; T_c describes the phase transition temperature between orientationally disordered and ordered phases; quantities A_0 and B are material constants; k_e is the representative elastic constant; and ∇_s is the surface gradient operator. It is important to note that the introduction of a single constant, k_e, assumes that bend and splay-type deformations in $\bar{n}$ are equally weighted in f_e. If the elastic terms are relatively negligible, then the equilibrium degree of ordering in the orientationally ordered phase is given by:

$$\lambda_{eq} = \lambda_0 \sqrt{-t}, \tag{10}$$

where $\lambda_0 = \sqrt{A_0/(2B)}$. The order parameter correlation length is estimated by:

$$\xi_b \sim \frac{\xi_0}{\sqrt{|t|}}, \tag{11}$$

and

$$\xi_0 = \sqrt{k_e/A_0}. \tag{12}$$

We define several dimensionless parameters. We scaled all the distances in terms of a characteristic linear size (R) of a structure; therefore, $\tilde{r} = r/R$, $\tilde{z} = z/R$, and $\tilde{\nabla}_s = R\nabla_s$, and we introduced dimensionless quantities $\tilde{K} = R^2 K$, $\tilde{H} = RH$, $\tilde{\kappa}_{q1} = R\kappa_{q1}$, $\tilde{\kappa}_{q2} = R\kappa_{q2}$, $t = (T - T_c)/T_c$, and $\tilde{f} = f/f_0$. Here,

$f_0 = k_e/R^2$ and κ_{qi} (where $i = 1,2$), stands for the geodesic curvatures of the i-th principal curvature. Because the meridians are geodesics, it follows that $\kappa_{q1} = 0$. Furthermore, we introduced the scaled order parameters $\tilde{\underline{Q}} = \underline{Q}/\lambda_0$, $\tilde{q}_0 = q_0/\lambda_0$, and $\tilde{q}_m = q_m/\lambda_0$. Then the corresponding dimensionless free energy density reads:

$$\tilde{f} = \left(\frac{R}{\xi_0}\right)^2 \left(tTr\tilde{\underline{Q}}^2 + \frac{1}{4}\left(Tr\tilde{\underline{Q}}^2\right)^2\right) + \frac{1}{2}\left|\tilde{\nabla}_s \tilde{\underline{Q}}\right|^2, \tag{13}$$

where

$$Tr\tilde{\underline{Q}}^2 = \tilde{q}_0^2 + \tilde{q}_m^2, \tag{14}$$

$$\left|\tilde{\nabla}_s \tilde{\underline{Q}}\right|^2 = \left(\tilde{q}_{0,s}^2 + \tilde{q}_{m,s}^2\right) + \frac{1}{\tilde{r}^2}\left(\tilde{q}_{0,\varphi}^2 + \tilde{q}_{m,\varphi}^2\right)$$
$$+ \left(\tilde{q}_0^2 + \tilde{q}_m^2\right)\psi + \frac{4\tilde{\kappa}_{q2}}{\tilde{r}}\left(\tilde{q}_0\tilde{q}_{m,\varphi} + \tilde{q}_{0,\varphi}\tilde{q}_m\right) \tag{15}$$

$$\psi = \tilde{H}^2 - 2\tilde{K} + 4\tilde{\kappa}_{q2}^2, \tag{16}$$

$$\tilde{K} = \frac{LN - M^2}{EG - F^2}, \tag{17}$$

$$\tilde{H} = \frac{EN + GL - 2FM}{2\left(EG - F^2\right)}, \tag{18}$$

$$\tilde{\kappa}_{q2} = -\frac{E_{,s}}{2E\sqrt{G}}. \tag{19}$$

The corresponding Euler–Lagrange equations are given by:

$$\frac{\partial}{\partial s}\left(\frac{\partial g}{\partial \tilde{q}_{0,s}}\right) + \frac{\partial}{\partial \varphi}\left(\frac{\partial g}{\partial \tilde{q}_{0,\varphi}}\right) - \frac{\partial g}{\partial \tilde{q}_0} = 0, \tag{20}$$

$$\frac{\partial}{\partial s}\left(\frac{\partial g}{\partial \tilde{q}_{m,s}}\right) + \frac{\partial}{\partial \varphi}\left(\frac{\partial g}{\partial \tilde{q}_{m,\varphi}}\right) - \frac{\partial g}{\partial \tilde{q}_m} = 0, \tag{21}$$

and

$$g = \tilde{f}\zeta, \tag{22}$$

where

$$\zeta = \tilde{r}\sqrt{\left(\tilde{r}_{,s}\right)^2 + \left(\tilde{z}_{,s}\right)^2} \tag{23}$$

stands for the Jacobian determinant. The equations were solved numerically using standard relaxation methods described in detail elsewhere.[22]